Atomic structure and adhesion of the Nb(001)∕α-Nb$_5$Si$_3$(001) interface: a first-principles study

Atomic structure and adhesion of the Nb(001)/α-Nb₅Si₃(001) interface: a first-principles study

Jia-Xiang Shang[1,3], Kun Guan[1] and Fu-He Wang[2]

[1] School of Materials Science and Engineering, Beihang University, Beijing 100191,
People's Republic of China
[2] Department of Physics, Capital Normal University, Beijing 100048,
People's Republic of China

E-mail: shangjx@buaa.edu.cn

Abstract
The density functional calculations have been performed to study the Nb(001) and
α-Nb₅Si₃(001) surfaces as well as the interface properties of Nb(001)/α-Nb₅Si₃(001). The
surface energy of the Nb(001) surface is about 2.25 J m^{-2}. The calculated cleavage energies of
bulk Nb₅Si₃ are 5.103 J m^{-2} and 5.787 J m^{-2} along (001) planes with the breaking of Nb–Si
and Nb–NbSi bonds, respectively. For the Nb(001)/α-Nb₅Si₃(001) models, the Nb atoms in the
interface region initially belonging to body centered cubic metal Nb are twisted to the position
of the Nb atom layer in Nb₅Si₃ and the interlayer distance is similar to that of bulk Nb₅Si₃ after
being fully relaxed. The ideal work of adhesion of the Nb(001)/Nb₅Si₃(001) interface is
calculated and compared to those of bulk Nb and Nb₅Si₃. The results show that the bulk Nb₅Si₃
has the largest work of adhesion, the bcc Nb ranks second and the interface ranks last.
Moreover, the Nb–Si bond is weaker than Nb–NbSi and Nb–Nb bonds in the interface, which
means that the Nb–Si bond in the interface is the most possible site for the micro-crack
generation when the stress is applied quasi-statically along the [001] direction. The densities of
states, Mulliken population and overlap population of the Nb(001)/α-Nb₅Si₃(001) interface are
also analyzed.

(Some figures in this article are in colour only in the electronic version)

1. Introduction

The refractory metal silicide-based alloys have been extensively studied as the candidate materials for the next generation of high temperature applications. Due to their high melting points and relatively low densities, they are expected to overcome the operating temperature barrier associated with the nickel-based superalloys. However, Nb₅Si₃ exhibits a limited capability of plastic deformation and poor ductility at ambient temperature. In order to overcome this frailty, the ductile metal Nb phase has been introduced to form the Nb_SS/Nb₅Si₃ *in situ* composites (Nb_SS: Nb solid solution), which have been studied [1–7] extensively. In these studies, the main purpose is to balance the ambient temperature toughness and high

temperature strength as well as oxidation resistance. The concept of brittle materials toughened by introducing a ductile phase was originally proposed by Krstic [8] and widely used to improve the fracture toughness of brittle materials [9–12]. The structure configuration and chemical bonding states of the interface between the reinforcement component and brittle material play an important role in the mechanical properties of the composites. The adhesion and debonding of the interface affect the toughness of materials greatly. The influence of ceramic–metal interface adhesion on crack growth resistance of ZrO₂–Nb ceramic matrix composites was investigated by first-principles calculation and high resolution transmission electron microscopy (HRTEM) [12]. In the study, the correlation between the work of adhesion of the interface and the mechanical properties was achieved. The toughness effects

---

[3] Author to whom any correspondence should be addressed.
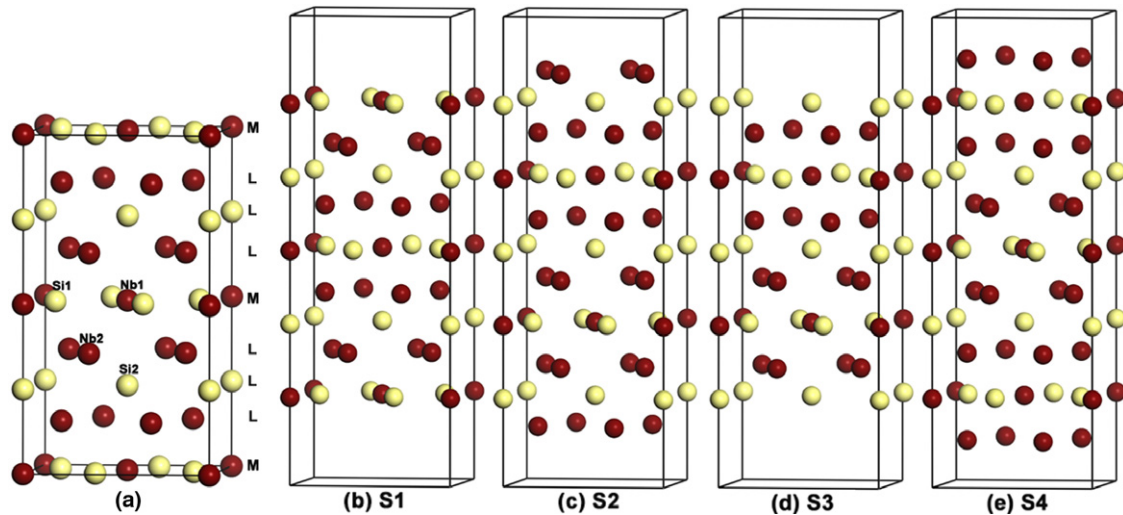
Figure 1. (a) Bulk α-Nb$_5$Si$_3$; (b)–(e) α-Nb$_5$Si$_3$(001) surface models. (b) NbSi(Nb) terminated denoted by S1; (c) Nb(Si) terminated denoted by S2; (d) Si(Nb) terminated denoted by S3; (e) Nb(NbSi) terminated denoted by S4.

were attributed mainly to crack bridging and crack deflection. This toughening mechanism is used for Nb$_5$Si$_3$ by introducing the ductile Nb phase to form Nb$_{SS}$/Nb$_5$Si$_3$ *in situ* composites; in these composites the Nb$_{SS}$ provides the toughness at ambient temperature and the intermetallic Nb$_5$Si$_3$ supplies strength at high temperature [1–7]. The plastic deformation of Nb$_{SS}$ and interface decohesion is responsible for high fracture toughness in this system [2, 7]. There are many investigations about the internal interface structure by HRTEM [12–15]. However, few experimental quantitative studies about interface adhesion have been carried out because of its difficulties. There are many theoretical calculations about the interface work of adhesion by the *ab initio* method [12, 16–21], which is used to discuss the mechanical properties of materials.

It is known the interfaces between metals and intermetallic compounds play a very important role in the room temperature toughness and the high temperature strength as well as the high temperature oxidation resistance. In order to improve the low temperature ductility and understand its mechanism, researchers have obtained the crystallographic orientation relationship between Nb$_{SS}$ and Nb$_5$Si$_3$ by electron backscatter diffraction analysis [22, 23]. However, the detailed interface structure of Nb/α-Nb$_5$Si$_3$ is hard to detect directly in the experiments. Fortunately, we can use first-principles calculations to determinate the structure and strength of the interface at the atomic scale. As the first step, we chose the Nb[100](001)/α-Nb$_5$Si$_3$[100](001) as our objective due to its perfect interfacial lattice matching in theory. The geometry and cohesion strength as well as the electronic structure of the Nb(001)/Nb$_5$Si$_3$(001) interface are investigated by density functional theory (DFT).

2. Calculation method and models

The DFT calculations presented in this paper are carried out with the Vienna *ab initio* simulation package (VASP) [24–26], employing projector augmented wave (PAW) pseudopotentials [27, 28] and the PW91 [29] generalized gradient approximation (GGA) exchange correlation functional. We tested kinetic-energy cutoff and k-point sampling convergence for all supercells and verified the accuracy of the computational methods by calculating the bulk properties of Nb and α-Nb$_5$Si$_3$. As a result of the convergence tests, we use the kinetic-energy cutoff of 400 eV. For the bulk calculations, models have been fully relaxed until the force of every atom is less than 0.01eV Å^{-1}. The calculated lattice constants of the body centered cubic (bcc) Nb is $a = 3.323$ Å, which agrees well with the experimental value $a = 3.30$ Å [30]. The calculated bulk modulus B_0 and cohesive energy of bcc Nb are 174.3 GPa and 7.09 eV/atom, which are consistent with the experimental values [30] (experimental values: 170.2 GPa and 7.57 eV/atom). The calculated lattice constants of α-Nb$_5$Si$_3$ are $a = 6.621$ Å, $c = 11.959$ Å and $c/a = 1.806$, which agree well with experimental values [31] and previous DFT results [32]. The calculated bulk modulus B_0 and cohesive energy of α-Nb$_5$Si$_3$ are 193 GPa and 6.837 eV/atom, respectively, but experimental values are not available.

As shown in figure 1(a), the unit cell of α-Nb$_5$Si$_3$ is stacked with atomic layers in the following order: MLLLMLLL (M and L denote the more close-packed and less close-packed layers, respectively) [32–34] along the c direction. It can be determined that there are two groups of niobium atoms (Nb1 and Nb2) and two groups of silicon atoms (Si1 and Si2) in the α-Nb$_5$Si$_3$ unit cell from their geometric position. We use Nb1 (Nb2) and Si1 (Si2) to denote the niobium and silicon atoms on the more (less) close-packed layers in the α-Nb$_5$Si$_3$ unit cell.

The Nb(001) surface was modeled by a slab of 4–11 atomic layers separated by a vacuum region of 15 Å. The Nb(001) surface calculations were done in 2×2 surface unit cells with $5 \times 5 \times 1$ Monkhorst–Pack k-points in the Brillouin zone. All the α-Nb$_5$Si$_3$(001) surfaces were modeled by a slab of 9 or 11 atomic layers separated by a vacuum region of 15 Å. The surface calculations were done in 1×1 surface unit cells with $5 \times 5 \times 1$ Monkhorst–Pack k-points in the Brillouin zone.
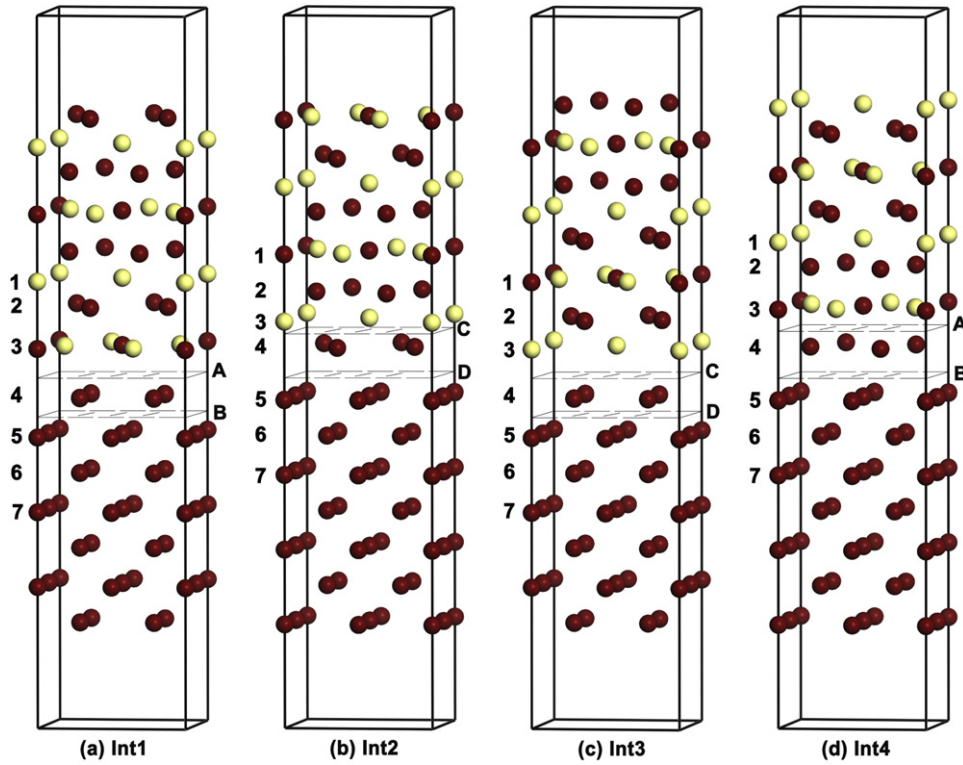
Figure 2. The four interface models of the Nb(001)/Nb$_5$Si$_3$(001), which are denoted by Int1, Int2, Int3 and Int4, respectively. The red (dark) and yellow (light) balls represent the Nb and Si atoms, respectively. The above eight-layer is α-Nb$_5$Si$_3$(001), the below seven-layer is Nb(001). A, B, C and D planes were assumed as the cleavage plane to calculate the interface work of adhesion.

The α-Nb$_5$Si$_3$ bulk has a D8$_1$ symmetry with a complicated stacking sequence. So the α-Nb$_5$Si$_3$(001) surface has four different terminal surfaces as shown in figures 1(b)–(e), where the four terminal surfaces: Nb and Si mixture NbSi(Nb), pure Nb(Si), pure Si(Nb) and pure Nb(NbSi) are denoted by S1, S2, S3 and S4, respectively. The letters in parentheses are the atoms in the second layer.

For Nb/Nb$_5$Si$_3$ interfaces, there are a number of ways for two surfaces to form an interface. According to the electron backscattering diffraction observation [22, 23], there are 11 kinds of crystallographic orientation relationships between Nb and α-Nb$_5$Si$_3$. We chose the Nb[100](001)/Nb$_5$Si$_3$[100](001) interface as our objective, which possesses a good matching. Our interface simulations use the bulk lattice constants, $2a[100]_{Nb} = 6.646$ Å and $a[100]_{\alpha-Nb5Si3} = 6.621$ Å. Based on these bulk lattice constants, the lattice misfit of the interface is 0.36%. We use the coherent interface in our calculations due to this small misfit.

Based on atomic structure of the Nb(001)/Nb$_5$Si$_3$(001) interface, there are four distinct interfacial stacking sequences to be considered. The four Nb(001)/Nb$_5$Si$_3$(001) interfaces are constructed by an eight-layer slab of α-Nb$_5$Si$_3$(001), a seven-layer slab of Nb(001) and a 15 Å vacuum layer. According to the terminations of the Nb$_5$Si$_3$(001) surface, four possible atomic stacking sequences are considered at the interface region in the interface systems: the NbSi(Nb), Nb(Si), Si(Nb) and Nb(NbSi) terminated surfaces are combined rigidly with an Nb(001) layer, which are denoted by Int1, Int2, Int3 and Int4, respectively. In order to accelerate the

convergence speed, at the first step of relaxation the two parts Nb$_5$Si$_3$(001) and Nb(001) are moved rigidly. The separation between Nb$_5$Si$_3$(001) and Nb(001) is determined by the energy minimization. The rigidly adjusted interface structures are shown in figures 2 (a)–(d). To discuss clearly, some of the atomic layers are labeled with numbers. At the second step of relaxation, only the atomic coordinates were allowed to relax until the force on each of the atoms was less than 0.01 eV Å^{-1}.

3. Surface properties

3.1. The Nb(001) surface

To determine the minimum thickness necessary for an Nb(001) surface, we have calculated the surface energy for slabs thickness from 4 up to 11 atomic layers. We find that the surface energy is converged to a dashed line in figure 3. The surface energy is converged to about 2.25 J m^{-2} for the thickness of Nb(001) being equal or larger than 5 atomic layers. The first interlayer spacing exhibits about 12% contraction, which is in agreement with theoretical [35, 36] and experimental results [37]. The calculated surface energy of Nb(110) is 2.03 J m^{-2}, which agrees well with other DFT results [35].

3.2. The α-Nb$_5$Si$_3$(001) surface

In order to understand the bond strength of Nb$_5$Si$_3$, the cleavage energy is calculated by two complementary parts
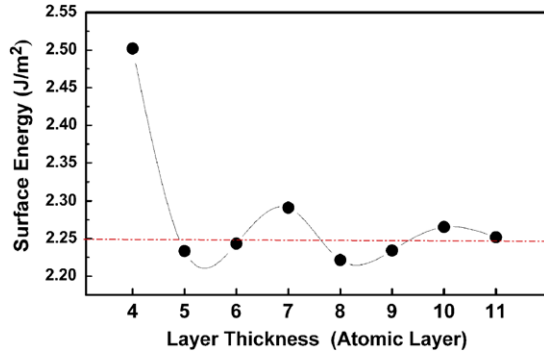
Figure 3. Surface energy of the Nb(001) (2 × 2) surface with different thickness (atomic layer).

Table 1. The cleavage energy and the bulk interlayer distance in α-Nb_5Si_3

Layer–layer	Cleavage energy (J m^{-2})	Interlayer distance (Å)
Nb–Si	5.103	1.216
Nb–NbSi	5.787	1.774

of the surfaces. The cleavage energy is defined as the energy to split the bulk into two complementary parts of the surfaces [38–40]:

$$E_{cl}^{X+Y} = \frac{1}{2S_0}(E_{slab}^{X} + E_{slab}^{Y} - nE_{Nb_5Si_3}^{bulk}). \quad (1)$$

E_{cl}^{X+Y} represents the cleavage energy. S_0 is the surface area of slab X or slab Y. The surface area of slab X is equal to that of slab Y. E_{slab}^{X} and E_{slab}^{Y} are the total energy of the two complementary surfaces which have been relaxed with fixed surface area. $E_{Nb_5Si_3}^{bulk}$ is the total energy of bulk Nb_5Si_3 of a unit cell and n is the total number of bulk units in the two slabs. In figure 1, S1 and S2, as well as S3 and S4, are two complementary surfaces, respectively. The cleavage energy and the interlayer distance between (001) planes in the bulk α-Nb_5Si_3 are listed in table 1.

From table 1, it can be seen that the cleavage energy between the Nb and Si plane is smaller (5.103 J m^{-2}) than that between the Nb and NbSi planes (5.787 J m^{-2}), though the interlayer distance between the Nb and Si planes (1.216 Å) is smaller than that between the Nb and NbSi planes (1.774 Å). It means that the interaction between the Nb and NbSi planes is stronger than that between Nb and Si planes. Therefore, it can be predicted that, when the tensile stress is applied quasi-statically along the [001] direction, the cleavage would be located in the Nb–Si bond in α-Nb_5Si_3.

We have investigated the surface energies of the clean $Nb_5Si_3(001)$ surface with different surface terminations as the functions of chemical potential of Si by DFT calculation [41]. It was found that the surface energy of the $Nb_5Si_3(001)$ surface with an Si surface termination is the lowest over the entire range of chemical potential of Si, which indicates that the most stable clean surface is an Si-terminated surface.

Interlayer relaxation can be evaluated by $\Delta = (d - d_0) \times 100/d_0$. Here d and d_0 are the interlayer distances of
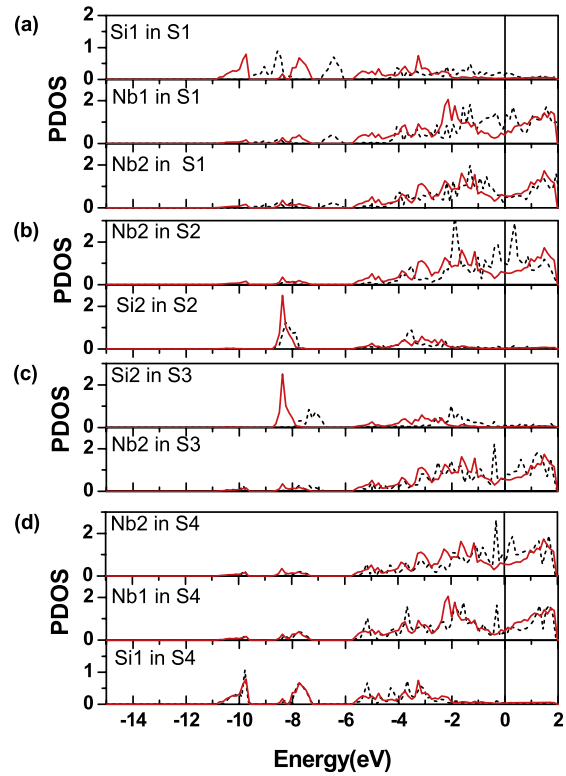
Figure 4. The projected density of states (PDOS) of the top two surface layers of the α-$Nb_5Si_3(001)$ surface with different terminations compared with that of the corresponding atoms in the bulk α-Nb_5Si_3 (solid red line). The black short dashed lines correspond to the PDOS of the top two layers surface of the surface models. (a) S1 with NbSi(Nb) termination; (b) S2 with Nb(Si) termination; (c) S3 with Si(Nb) termination and (d) S4 with Nb(NbSi) termination. The Fermi level is shifted to zero.

Table 2. Interlayer relaxations Δ_{12}, Δ_{23} and Δ_{34} of the α-$Nb_5Si_3(001)$ surface with different surface terminations, given as a percentage of the bulk spacing.

	Models			
	S1	S2	S3	S4
Δ_{12}	0.8	−17.4	−20.3	−7.5
Δ_{23}	−3.4	−2.6	−0.7	2.1
Δ_{34}	0.8	2.7	−0.3	−0.7

relaxed surface and bulk materials, respectively. The calculated results are listed in table 2. The surface relaxations with different terminations are different. Nb(Si) and Si(Nb) surface relaxations are very large, which contract about 17% and 20%, respectively. However, the NbSi mixture surface layer has only a little expansion (less than 1%) and the surface relaxation of the Nb(NbSi) surface is just contracted by about 7.5%, which is much smaller than that of the Nb(Si) or Si(Nb) surface.

Figure 4 shows the projected density of states (PDOS) of the top two layers of the α-$Nb_5Si_3(001)$ surface with different terminations compared with that of the corresponding atoms in the bulk α-Nb_5Si_3. For the S2 and S4 models, both surfaces are terminated by Nb atoms, the low energy levels at about −11 and −7.0 eV change slightly, while the high energy levels of Nb atoms at about −5.5–0 eV are shifted to the higher energy

Table 3. Interlayer distance (in Å) in the interface region of the four fully optimized interface models.

Interlayer distance	Models			
	Int 1	Int 4	Int 2	Int 3
d_{1-2}	1.205	1.206	1.788	1.805
d_{2-3}	1.797	1.788	1.204	1.204
d_{3-4}	1.779	1.784	1.181	1.183
d_{4-5}	1.856	1.841	1.824	1.832
d_{5-6}	1.644	1.635	1.648	1.657

Table 4. The work of interface adhesion W_{ad} (in J m^{-2}) of different interface models.

Models	Cleaving planes	W_{ad} (J m^{-2})
Int1	B (Nb/Nb)	4.29
Int4	B (Nb/Nb)	4.36
Int2	D (Nb/Nb)	4.30
Int3	D (Nb/Nb)	4.28
Int2	C (Nb/Si)	3.81
Int3	C (Nb/Si)	3.99
Int1	A (Nb/NbSi)	4.47
Int4	A (Nb/NbSi)	4.34

level compared with that of bulk α-Nb$_5$Si$_3$. While for S1 (terminated by Nb and Si) and S3 (terminated by Si) models, it was found that the energy levels of surface and subsurface atoms are all shifted to the higher energy at an entirely energy region compared with that of corresponding bulk atoms, which is the effect of Si atoms at the surface layer. The strong covalent interaction exists between Si and its neighboring atom in the bulk Nb$_5$Si$_3$ [33]. It is because of the unsaturated chemical bonds and the unbalanced atomic interactions caused by the decrease of neighboring atoms, that the energy levels of the surface atoms shift to higher values. It is easy to understand that dangling bonds exist on the surfaces terminated by the Si atomic layer or Nb–Si mixing layer, whereas metallic bonds are formed if the surface is terminated by pure Nb atoms. As for S2 and S3 surfaces, we attribute their largest interlayer relaxations to the weak bonds perpendicular to the surfaces.

4. Interface properties

4.1. Atomic structures

As mentioned in section 2, the geometries of the four interface models are optimized by two steps. At the first step, the atoms in the two parts α-Nb$_5$Si$_3$ and Nb are moved rigidly, the relative position of each atom fixed in its own part. As shown in figures 2(a) and (c), the Nb(4) atomic layer belongs to the Nb part, while the Nb(4) atomic layer belongs to the α-Nb$_5$Si$_3$ part as shown in figures 2(b) and (d). After the second step of the optimization, i.e. the interface structure is fully optimized, the Nb(4) atomic layer in figures 2(a) and (c) in the Int1 and Int3 models is twisted about 13.9° and similar to the Nb atoms in the counterpart layer of the α-Nb$_5$Si$_3$. (The normal twist angle is 18.6° in α-Nb$_5$Si$_3$.) So that the Nb(4) layer is almost changed to be one layer of the α-Nb$_5$Si$_3$.

Interlayer distances are important for us to discuss the interface structure. The calculated interlayer distances for optimized interface models are presented in table 3. It was found that the interlayer spacing of Int1 and Int4 is very similar. So Int1 and Int4 are the same kind of interface. The interlayer distances of Int2 and Int3 are very similar, which is another kind of interface. The interlayer distance between (001) planes in the bulk Nb is 1.661 Å and the interlayer distances in bulk α-Nb$_5$Si$_3$ are 1.774 Å and 1.216 Å, respectively (see table 1). After being fully optimized, the interlayer distances d_{4-5} for Nb–Nb in the interface region are more than 1.82 Å for all four interface models, which is larger than that in the bulk Nb. The values of other interlayer distances are almost the same as

those in the bulk Nb and α-Nb$_5$Si$_3$. The Nb(4) layer in the Int1 and Int3 interface models should be discussed again. Before being fully optimized, the Nb(4) atomic layer belongs to the metal Nb, and the interlayer distance d_{4-5} is 1.661 Å. After being fully optimized, the interlayer distance d_{4-5} between Nb layers is enlarged, while the interlayer distance d_{3-4} is almost the same as those in the bulk α-Nb$_5$Si$_3$. As a result, the Nb(4) atomic layer in the Int1 or Int3 interface model is changed to be one layer of Nb$_5$Si$_3$. This is because Nb is more stable in the bulk α-Nb$_5$Si$_3$ than in the bulk Nb. This situation was also found in the Al/Al$_2$O$_3$ interface [17].

4.2. The work of interface adhesion

The ideal work of adhesion W_{ad} of an interface is defined as the energy needed per unit area to reversibly separate an interface into two free surfaces, which is the key to predict the mechanical properties of an interface. W_{ad} can be obtained by [12, 16–21]

$$W_{ad} = (E_{slab}^{A} + E_{slab}^{B} - E_{slab}^{A/B})/A_{i} \tag{2}$$

where E_{slab}^{A} and E_{slab}^{B} represent the total energy of a relaxed, isolated slab A and slab B model. $E_{slab}^{A/B}$ denotes the total energy of a slab A/B system. A_{i} is the interface area.

According to the atomic structure of the interface region, we can class the interface models into two kinds: one is the NbSi–Nb interface region such as Int1 and Int4 models, the other kind is the Si–Nb interface region such as Int2 and Int3 models. In order to evaluate the work of interface adhesion, we assume the interface cleaves at NbSi–Nb (A) and Nb–Nb (B) in the interface region for Int1 and Int4 models, and at Si–Nb (C) and Nb–Nb (D) in the interface region for Int2 and Int3 models. The calculated work of interface adhesion with different cleavage planes for different interface models is presented in table 4. It can be seen that the values of the work of interface adhesion cleaving between Nb and Nb layers for all four models are very similar (from 4.28 to 4.36 J m^{-2}), which is a little smaller than that of bulk Nb (4.50 J m^{-2}) cleaving along (001) planes. This corresponds to the enlarged interlayer distances d_{4-5} in the interface region compared with the value of bulk Nb. As a result, the interaction between Nb atoms in these two layers is weakened. The values of the works of interface adhesion cleaving between Nb and Si layers in the interface region are 3.81 J m^{-2} and 3.99 J m^{-2} for Int2 and Int3 models, respectively, which are much smaller than the cleavage

energy 5.103 J m^{-2} of bulk Nb–Si (see table 1). The interlayer distances in the interface region between Nb and Si are almost the same: 1.181 Å and 1.183 Å for Int2 and Int3 models, respectively. For Nb–NbSi cleavage, the cleavage energy is 5.787 J m^{-2} (see table 1) in the bulk Nb_5Si_3. However, the values of the work of interface adhesion cleaving between Nb and NbSi layers are only 4.47 J m^{-2} for the Int1 model and 4.34 J m^{-2} for the Int4 model, which is much smaller than the cleavage energy of bulk Nb_5Si_3. The interlayer distance between Nb and NbSi in the interface region in the Int1 model is 1.779 Å, which is similar to that of the Int3 model as well as bulk Nb_5Si_3 (1.774 Å). The work of interface adhesion in all the interface models is weaker than that of bulk Nb_5Si_3 and bulk Nb along the (001) plane. The bonding between Nb and Si layers in the interface region is the weakest. The Nb–Si bond in the interface region is the most probable site for micro-crack generation when the stress is applied quasi-statically.

4.3. Density of states

As discussed above, the interfaces can be classified into two kinds. In the following, Int1 and Int3 interface models are chosen as typical models to discuss the electronic structure of the two kinds of interfaces. Figure 5 presents the density of states (DOS) of atoms in the interface region of the Int1 model compared with that of the corresponding atoms in bulk Nb_5Si_3 and the central atom Nb(7) in metal Nb. It can be seen that the DOS of Nb(7) in the center of the metal Nb is different from that of the Nb atom in the bulk Nb_5Si_3. The electronic states of Nb(7) are distributed in the energy range from -4.8 to 0 eV, whereas the energy states of Nb1 and Nb2 in the bulk Nb_5Si_3 are distributed from -11 to -9.5 eV and from -8.5 to -7.3 eV as well as from -5.8 to 0 eV. In the interface region, there is a set of new low energy states on the metal Nb(4) atoms in the -10.5 to -9.5 eV range and -8.0 to -7.0 eV range due to overlap with the states of Si(3) and Nb(3) atoms. The DOS of the Nb(4) atom shows more like that of the Nb2 atom in bulk α-Nb_5Si_3, which is consistent with the result of the atomic structure analysis. For the atoms Nb(3) and Si(3), the DOSs are very similar to that of corresponding atoms in bulk Nb_5Si_3, but the energy levels are shifted upward slightly.

Figure 6 shows the DOS of another kind of interface model Int3. At the interface layer, there are some overlaps between the hybridized states on Nb(4) in the -8.7 to -7.8 eV and -5.2 to -1.0 eV ranges with the electron states of Si(3), suggesting a covalent bonding. The low energy states on the interfacial Nb layer involve Nb(4) and Nb(5) atoms. It can also be found that there are more electronic states in the -1.2–0 eV range for the Nb(4) atom relative to the DOS for the Nb2 atom in bulk Nb_5Si_3.

Comparing figure 5 with figure 6, it can be found that the main difference between Int1 and Int3 models is that there are more overlap states between Si(3) or Nb(3) and Nb(4) atoms in the Int1 model than between Si(3) and Nb(4) in the Int3 model. For the Int1 model, the overlapping states between Si(3) or Nb(3) and Nb(4) atoms appear at about from -10.5 to -9.5 eV, from -8.0 to -7.0 eV and from -5.5 to 0 eV energy ranges. However, for the Int3 model, the interaction between Si(3) and
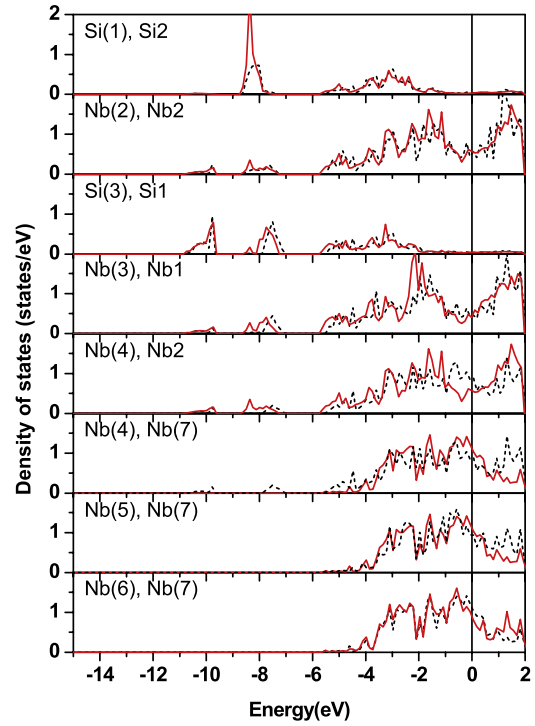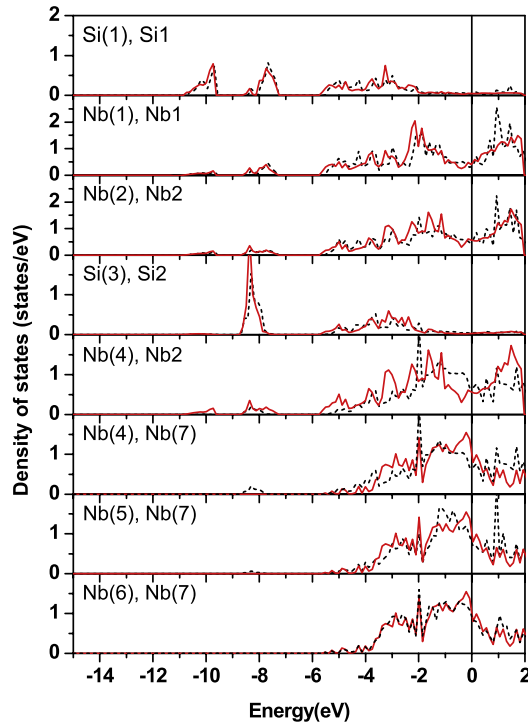

Figure 5. Density of states of selected atoms for the Int1 model. Black short dashed lines correspond to the DOS of the selected atoms for the Int1 model and red solid lines correspond to the DOS of the corresponding atoms in bulk Nb_5Si_3 (Nb1, Nb2, Si1 and Si2) or the central Nb(7) atom in metal Nb. Fermi energy is shifted to zero. Si(1), Nb(2), Si(3), Nb(3), Nb(4), Nb(5), Nb(6) and Nb(7) correspond to the atoms in different layers labeled in figure 2(a).

Nb(4) exists at energy ranges from -8.7 to -7.8 eV, and from -5.2 to -1.0 eV. This means that the interaction between Si(3) or Nb(3) and Nb(4) for the Int1 model is stronger than that between Si(3) and Nb(4) for the Int3 model, which is consistent with the previous results of the interface work of adhesion.

4.4. Mulliken charge and overlap analysis

In order to analyze the charge transfer and the relative strength of a given bond, we calculated the Mulliken charge [42] and overlap population [43, 44] using the CASTEP [45] electronic structure code. It is widely accepted that a large value of the overlap population indicates a covalent bond [43, 44]. The larger the overlap population is, the stronger the covalence bond is. The Mulliken charge and overlap population of the Int1 and Int3 models are calculated. For comparison, we also performed calculations on the bulk Nb and bulk Nb_5Si_3. The calculated results are listed in table 5.

For the Int1 model, 0.14e are transferred from the metal Nb slab to the Nb_5Si_3. By summing the charges layer by layer, it is found that lost charges are mainly from Nb(5) atoms, while Nb(4) and Si(3) atoms gain the charges. For the central layer of metal Nb, Nb(6) and Nb(7) atoms exhibit smaller charges $-0.01e$ and $+0.01e$, respectively. It can be found that the overlap population of Si(3)–Nb(4) is almost the same as that in bulk Nb_5Si_3. However, the overlap population of the Nb(4)– Nb(5) bond is only 0.07 (the overlap population is 0.26 for bcc

Figure 6. Density of states of selected atoms for the Int3 model. Black short dashed lines correspond to the DOS of the selected atoms for the Int3 model and red solid lines correspond to the DOS of corresponding atoms in bulk Nb_5Si_3 (Nb1, Nb2, Si1 and Si2) or the central Nb(7) atom in Nb. Si(1), Nb(1), Nb(2), Si(3), Nb(4), Nb(5), Nb(6) and Nb(7) atoms correspond to the atoms in different layers labeled in figure 2(c). The Fermi energy is shifted to zero.

Nb), which indicates that the covalent or metallic component is decreased for the bond.

For the Int3 model, there is 0.06*e* net change transferred from the metal Nb slab to the Nb_5Si_3 slab. The charges lost by the metal Nb slab come mainly from the interfacial Nb(4) layer. The Nb(4) layer is mainly responsible for the charge transfer with a loss of 0.07*e*; the Nb(5) atom gains 0.04*e*. For the central layer of metal Nb, Nb(6) and Nb(7) atoms exhibit a smaller charge of −0.02*e* and +0.02*e*, respectively. The overlap population analysis of the Int3 model further confirms that the interfacial Si(3)–Nb(4) bond is very similar to that of the bulk Nb_5Si_3. The overlap population of the Nb(4)–Nb(5) bond is 0.34, which is larger than that of bulk bcc Nb (the overlap population is 0.26 for bcc Nb). This indicates that there is some degree of covalent component in the Nb(4)–Nb(5) bond. Comparing the results of Int1 with that of Int3, it is found that the electrostatic interaction of the Int1 model is stronger than that of Int3. Though the overlap population of Si(3)–Nb(4) in Int1 is almost the same as in Int3, electronic overlapping states in Int1 lie in the lower energy level than that in Int3. (This can be seen in figures 5 and figure 6.) This indicates that the covalent interaction of the Si(3)–Nb(4) bond in Int1 is stronger than that of Si(3)–Nb(4) in the Int3 model.

5. Conclusion

In summary, we have presented a density functional theory study of Nb(001) and α-Nb_5Si_3(001) surface properties as

Table 5. Mulliken charges and overlap population for the optimized interface Int1 and Int3 models compared with the bulk metal Nb and bulk α-Nb_5Si_3. Mulliken charge is the difference in valence electron number of the atom in the given model and the free atom. Positive charge means the atom loses electrons; negative charge means the atom gains electrons. Nb1, Si1, Nb2 and Si2 atoms of bulk α-Nb_5Si_3 correspond to the atoms labeled in figure 1(a).

	Int1	Int3	Bulk α-Nb_5Si_3	Bulk Nb
Atom		Mulliken charges		
Nb(1)	—	−0.02	Nb1: −0.03	
Si(1)	−0.08	−0.08	Si1: −0.06	
Nb(2)	+0.08	+0.09	Nb2: +0.05	
Si(3)	−0.10	−0.10	Si2: −0.07	
Nb(4)	−0.03	+0.07		
Nb(5)	+0.05	−0.04		
Nb(6)	−0.01	−0.02		
Nb(7)	+0.01	+0.02		
Bond		Overlap population		
Nb(2)–Si(3)	0.30	0.24	Nb1–Si2: 0.30	
Si(3)–Nb(4)	0.28	0.27	Nb2–Si2: 0.27	
Nb(4)–Nb(5)	0.07	0.34	Nb1–Si1: 0.22	Nb–Nb: 0.26

well as the interface properties of Nb(001)/α-Nb_5Si_3(001) by the Vienna *ab initio* simulation package (VASP). The surface energy of Nb(001) is about 2.25 J m^{-2} and the first interlayer spacing exhibits about 12% contraction, which is in agreement with the experimental result. To investigate the bond strength of bulk Nb_5Si_3, the four surface models are constructed. Based on the surface calculation, the calculated cleavage energies of bulk Nb_5Si_3 are 5.103 and 5.787 J m^{-2} for Nb–Si and Nb–NbSi bonds along the (001) plane. The four Nb(001)/α-Nb_5Si_3(001) interface models were investigated. Moreover, for the Si-terminated and NbSi-terminated interface models, the Nb atoms in the interface region initially belonging to metal Nb are twisted 13.9° and the interlayer distance is similar to that of bulk Nb_5Si_3. Therefore, the interfacial Nb atoms become the part of Nb_5Si_3. These Nb atoms present the new electronic states at lower energy level, which appears in the bulk Nb_5Si_3 and does not appear in bulk bcc metal Nb. The ideal work of adhesion of the Nb(001)/α-Nb_5Si_3(001) interface is calculated and compared with that of bulk Nb and bulk Nb_5Si_3. It is found that the interfacial Nb–Si bond has the smallest ideal work of adhesion, the bulk Nb_5Si_3 has the largest ideal work of adhesion and bcc Nb ranks the second. The electronic properties including density of states, Mulliken charge and overlap population are also discussed. From the analysis of electronic structure, it can be found that the electrostatic interaction of NbSi-terminated interface is stronger than that of Si-terminated interface; in the interface region, the covalent interaction between Si and Nb for NbSi-terminated interface model is stronger than that between Si and Nb for the Si-terminated interface model.

Acknowledgments

References

[1] Kim J H, Tabaru T, Hirai H, Kitahara A and Hanada S 2003 *Scr. Mater.* **48** 1439

[2] Kim W Y, Tanaka H, Kasama A and Hanada S 2001 *Intermetallics* **9** 827

[3] Kim W Y, Tanaka H and Hanada S 2002 *Intermetallics* **10** 625

[4] Kim W Y, Yeo I D, Ra T Y, Cho G S and Kim M S 2004 *J. Alloys Compounds* **364** 186

[5] Li W, Yang H B, Shan A D, Zhang L T and Wu J S 2006 *Intermetallics* **14** 392

[6] Kim J H, Tabaru T, Sakamoto M and Hanada S 2004 *Mater. Sci. Eng.* A **372** 137

[7] Li Z and Peng L M 2007 *Acta Mater.* **55** 6573

[8] Krstic V D 1993 *Phil. Mag.* **48** 695

[9] Flinn B D, Ruhle M and Evans A G 1989 *Acta Metall. Mater.* **37** 3001

[10] Zimmermann A, Hoffman M, Emmel T, Gross D and Rodel J 2001 *Acta Mater.* **49** 3177

[11] Sbaizero O, Pezzotti G and Nishida T 1998 *Acta Mater.* **46** 681

[12] Bartolome J F, Beltran J I, Gutierrez-Gonzalez C F, Pecharroman C, Munoz M C and Moya J S 2008 *Acta Mater.* **56** 3358

[13] Mi S B, Jia C L, Zhao Q T, Mantl S and Urban K 2009 *Acta Mater.* **57** 232

[14] Yang Z, Chen J, He L, Cong H and Ye H 2009 *Acta Mater.* **57** 3633

[15] Luysberg M, Heidelmann M, Houben L, Boese M, Heeg T, Schubert J and Roeckerath M 2009 *Acta Mater.* **57** 3192

[16] Siegel D J, Hector L G Jr and Adams J B 2002 *Phys. Rev.* B **65** 085415

[17] Raynolds J E, Smith J R, Zhao G L and Srolovitz D J 1996 *Phys. Rev.* B **53** 13883

[18] Zhang W and Smith J R 2000 *Phys. Rev.* B **61** 16883

[19] Liu W, Li J C, Zhang W T and Jiang Q 2006 *Phys. Rev.* B **73** 205421

[20] Beltran J I and Munoz M C 2008 *Phys. Rev.* B **78** 245417

[21] Liu Y and Szlufarska I 2009 *Phys. Rev.* B **79** 094109

[22] Miura S, Aoki K, Saeki Y, Ohkubo K and Mishima Y 2005 *Metall. Mater. Trans.* A **36** 489

[23] Miura S, Ohkubo K and Mohri T 2007 *Intermetallics* **15** 783

[24] Kresse G and Hafner J 1993 *Phys. Rev.* B **48** 13115

[25] Kresse G and Furthmuller J 1996 *Phys. Rev.* B **54** 11169

[26] Kresse G and Furthmuller J 1996 *Comput. Mater. Sci.* **6** 15

[27] Blöchl P E 1994 *Phys. Rev.* B **50** 17953

[28] Kresse G and Joubert D 1999 *Phys. Rev.* B **59** 1758

[29] Perdew J P, Chevary J A, Vosko S H, Jackson K A, Pederson M R, Singh D J and Fiolhais C 1992 *Phys. Rev.* B **46** 6671

[30] Kittle C 1971 *Introduction to Solid State Physics* 4th edn (New York: Wiley)

[31] *Natl. Bur. Stand. (US)* 1978 (*Monograph No. 25*) (Washington, DC: US GPO) p 43

[32] Chen Y, Shang J X and Zhang Y 2007 *J. Phys.: Condens. Matter* **19** 016215

[33] Chen Y, Shang J X and Zhang Y 2007 *Intermetallic* **15** 1558

[34] Chen Y, Shang J X and Zhang Y 2007 *Phys. Rev.* B **76** 184204

[35] Kwon S K, Nabi Z, Kádas K, Vitos L, Kollár J, Johansson B and Ahuja R 2005 *Phys. Rev.* B **72** 235423

[36] Fang B S, Lo W S, Chien T S, Leung T C, Lue C Y, Chan C T and Ho K M 1994 *Phys. Rev.* B **50** 11093

[37] Pan B and Hu Z 1990 *J. China Univ. Sci. Technol.* **20** 208

[38] Zhang H Z and Wang S Q 2007 *Acta Mater.* **55** 4645

[39] Heigets E, Goddard W A, Kotomin E A, Eglitis R I and Borstel G 2004 *Phys. Rev.* B **69** 035408

[40] Bottin F, Finocchi F and Noguera C 2003 *Phys. Rev.* B **68** 035418

[41] Liu S Y, Shang J X, Wang F H, Liu S, Zhang Y and Xu H B 2009 *Phys. Rev.* B **80** 085414

[42] Mulliken R S 1955 *J. Chem. Phys.* **23** 1833

[43] Segall M D, Pickard C J, Shah R and Payne M C 1996 *Mol. Phys.* **89** 571

[44] Segall M D, Shah R, Pickard C J and Payne M C 1996 *Phys. Rev.* B **54** 16317

[45] Segall M D, Lindan P L D, Probert M J, Pickard C J, Hasnip P J, Clark S J and Payne M C 2002 *J. Phys.: Condens. Matter* **14** 2717